Nanoparticles in SiH4-Ar plasma: Modelling and comparison with experimental data

B. F. Gordiets, M. J. Inestrosa-Izurieta, A. Navarro, and E. Bertran

Citation: J. Appl. Phys. **110**, 103302 (2011); doi: 10.1063/1.3658249
View online: http://dx.doi.org/10.1063/1.3658249
View Table of Contents: http://jap.aip.org/resource/1/JAPIAU/v110/i10
Published by the American Institute of Physics.

Nanoparticles in SiH_4-Ar plasma: Modelling and comparison with experimental data

B. F. Gordiets,[1,a)] M. J. Inestrosa-Izurieta,[2] A. Navarro,[3] and E. Bertran[2]
[1]*Lebedev Physical Institute of Russian Academy of Sciences, Leninsky Prospect 53, 119991 Moscow, Russia*
[2]*FEMAN Group, IN2UB, Departament de Fisica Aplicada i Optica, Universitat de Barcelona, Marti i Franques 1, E08028 Barcelona, Spain*
[3]*Universitat Politècnica de Catalunya, Terrassa, Spain*

(Received 28 July 2011; accepted 1 October 2011; published online 17 November 2011)

Experimental and theoretical investigations for growth of silicon nanoparticles (4 to 14 nm) in radio frequency discharge were carried out. Growth processes were performed with gas mixtures of SiH_4 and Ar in a plasma chemical reactor at low pressure. A distinctive feature of presented kinetic model of generation and growth of nanoparticles (compared to our earlier model) is its ability to investigate small "critical" dimensions of clusters, determining the rate of particle production and taking into account the influence of SiH_2 and Si_2H_m dimer radicals. The experiments in the present study were extended to high pressure ($\geq$20 Pa) and discharge power ($\geq$40 W). Model calculations were compared to experimental measurements, investigating the dimension of silicon nanoparticles as a function of time, discharge power, gas mixture, total pressure, and gas flow. © *2011 American Institute of Physics*. [doi:10.1063/1.3658249]

I. INTRODUCTION

Nanoparticles, which are generated in the gas phase of plasma chemical reactors and deposited onto thin films, affect different characteristics of these films (mechanical, optical, and electrical). A current problem of nanotechnology is the generation of nanoparticles with desirable composition and dimension. To this end, one such task is the investigation of Si nanoparticles, which are often studied using plasma chemical reactors at low pressure (10 to 100 Pa), and radio frequency (RF) discharge in pure silane or gas mixtures such as Ar-SiH_4 and He-SiH_4 (see, for example, the book[1]). Detailed experimental investigations of Si particle growth have been performed,[2–18] while theoretical studies of Si nanoparticle growth have also been carried out, developing both complex[19–22] and relatively simple[23–28] models. However, direct comparisons of experimental and theoretical results have not been shown in most cases. Important characteristics of nanoparticle kinetics (critical "dimension" n^* and rate for particle formation J_{n^*}) have been introduced and investigated.[26–28] In addition, a quantitative comparison and interpretation of experiments[2–5] investigating the generation and growth of Si nanoparticles in SiH_4-Ar plasma has been achieved. However, these experiments[2–5] were conducted only at one low discharge power (10 W), one low gas pressure (15.6 Pa), and one gas flow rate (30 sccm). Indeed, our previously reported model described these conditions (low pressure and power).[26–28]

Our aim here is to extend our earlier kinetic model[26–28] to describe the formation and growth of Si nanoparticles in SiH_4-Ar plasma at relatively high pressures ($\geq$20 Pa) and discharge powers ($\geq$40 W). For that, detailed measurements of Si nanoparticle dimensions were carried out at Barcelona University in a low pressure chemical vapour deposition reactor. Thus, particle diameter was determined as a function of process parameters like time (during particle growth), discharge power, gas pressure, gas flow rate, and relative inlet concentration of SiH_4.

II. EXPERIMENTAL DETAILS

The schematic view of our experimental set is given in Fig. 1. The RF capacitive discharge (frequency 13.56 MHz) was carried out in a rectangular box with dimensions $19 \times 19 \times 4$ cm^3. One of the lateral sides (with dimension 19×4 cm^2) was open (for gas outlet) and the opposite side had a narrow slit (with dimension 19×0.1 cm^2) 1 cm high (for gas inlet). Other sides with dimensions 19×4 cm^2 were closed. The distance between electrodes was 4 cm and the cathode was at the roof of the discharge box. All the surfaces were connected to the anode, and the cathode was placed on top of the box with dimension 19×19 cm^2.

The SiH_4-Ar gas mixture with controlled fixed gas flow rate entered the discharge box through the gas inlet narrow slit. The discharge box was placed into a large chamber, where the pressure and composition of the investigated SiH_4-Ar gas mixture was controlled. The discharges were performed as a series of pulses with constant duration in the range of 0.01 to 1.0 s and with a "discharge-off" period higher than the discharge resident time (which was dependent on gas flow rate and pressure, 0.05 to 0.8 s). During each "discharge-on" pulse, silicon nanoparticles were generated, then grown and then became negatively charged. Practically all particles remained electrically retained by the plasma sheath in the discharge region due to their negative charge. During the period of discharge-off, the electric sheath disappeared. However, independently of the duration of discharge-on pulse, both neutral and negatively charged particles escaped from the discharge area, carried by the gas flow during the time of residence. Outside the region of the

a)Electronic mail: bgordiets@rambler.ru.

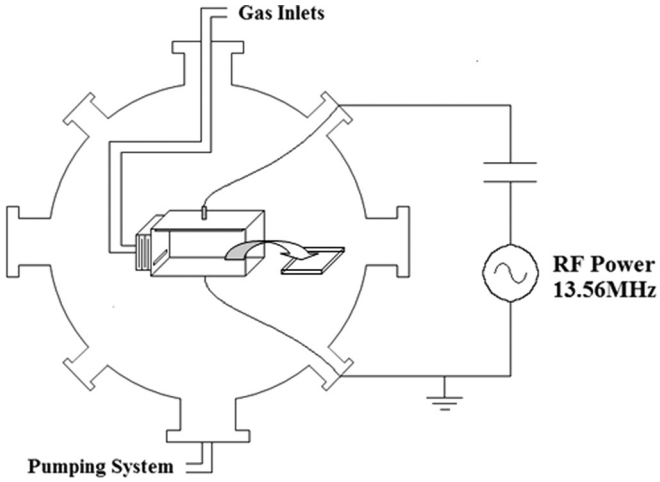

FIG. 1. Schematic view of our experimental setup including the vacuum chamber and the reaction chamber inside.

discharge, the particles quickly lost their negative charge and were deposited onto the out-of-the-box platform due to diffusion. These deposited particles had an average dimension and a distribution in sizes that depended on the following discharge parameters: duration of discharge-on, discharge power, gas pressure, gas flow rate, and inlet gas composition.

III. KINETIC MODEL FOR THE FORMATION AND GROWTH OF SI NANOPARTICLES AT RELATIVELY HIGH GAS PRESSURE AND DISCHARGE POWER

To describe the formation and growth of Si nanoparticles at high pressure and power, we implemented some changes to the previous model.[26–28] The main input parameters considered here were the discharge geometry, inlet gas composition (that is the relative inlet concentration X_{SiH_4} of SiH_4 molecules in the SiH_4–Ar mixture), gas pressure p (Pa), electrical power P (W) absorbed at the discharge zone, and gas flow rate Q (sccm) in the discharge zone. The main output features provided by the model were: the concentration of nanoparticles N_p (cm^{-3}) and their average diameter D_p (nm) or "dimension" $\langle n\rangle$ (average number of monomers in the particles). Other important characteristics were the concentration of the main monomers (radicals SiH_3 and SiH_2), electron density N_e (cm^{-3}) and electron temperature T_e (eV), positive ion density $N^+(cm^{-3})$, gas and ion temperatures T_g and T_i (K), relative fractions of neutral and charged particles, and average particle charge $\langle Z\rangle$. The model is, in fact, zero-dimensional and discharge geometry only determines discharge volume and surface as well as resident time and probabilities of diffusion losses for different species.

The formation of clusters and nanoparticles in molecular plasmas can be described as the result of dissociation of SiH_4 and related molecules. In our case, plasma electrons and metastable Ar* atoms are the main contributors to this dissociation. Hence, different radical-monomers and small-size clusters, mainly neutral and negatively charged, can be formed. Nanoparticles are created by the attachment of monomers to the clusters. Due to the attachment processes, nanoparticles continue to grow in size and their concentrations may attain a certain maximal value. To describe such processes, we will start from the reported basic equations[26–28] that will be modified according to the conditions of the present study.

Here, for simplicity, we will only consider α-regime of RF discharges, when electrons with high energy (≥15 eV) have low concentration and do not influence positively charged ion concentrations and nanoparticle charge. In this case (for zero-dimensional model), the obtained equation from our previous studies,[26,27] for the concentration of nanoparticles with dimension $\langle n\rangle$ in the discharge zone, can be simplified to

$$\frac{dN_p}{dt} \approx J_{n*} - W^{tot}_{\langle n\rangle} \times f_0 \times N_p - \frac{1}{\tau_{res}} \times N_p - (N_p)^2 \times f_0 \times \left[k^{00}_{\langle n\rangle} \times f_0 + k^{0-}_{\langle n\rangle} \times f_-\right]. \quad (1)$$

The first term $J_{n*}(cm^{-3}\ s^{-1})$ on the right-hand side of this equation is the rate of nanoparticle production. The second and third terms describe the losses of particles due to diffusion and escape processes by the gas flow from the discharge region. These processes are described by probabilities $f_0 \times W^{tot}_{\langle n\rangle}$ and $1/\tau_{res}$, respectively (τ_{res} is the residence time for gas and particles in the discharge zone). The last term describes coagulation due to collisions of neutral particles with neutral and negatively charged particles with the rate coefficients $k^{00}_{\langle n\rangle}$ and $k^{0-}_{\langle n\rangle}$, respectively. This term is obtained with the assumption that particle dimension distribution is a δ-function. Parameters f_0 and f_- are the relative fractions of neutral and negatively charged particles, respectively, with $f_- \approx 1 - f_0$. It is important to note that all the terms on the right-hand side of Eq. (1) refer to processes performed in the discharge region. However, for the used geometry of our discharge (see Fig. 1), all neutral and negatively charged particles will escape from the discharge zone dragged by the gas flow, at $t > \tau_{res}$, outside of the discharge region. Due to the fast recombination of positive ions with electrons and negatively charged particles, the negatively charged particle concentration falls instantly so that most of the particles become neutral. Therefore, in the framework of our simple zero-dimensional kinetic model, in Eq. (1) at $t > \tau_{res}$, it is necessary to consider $f_0 = 1$ and neglect the term $1/\tau_{res}$.

The equation for the average particle dimension, $\langle n\rangle$, was also obtained in our previous studies[26,27] as

$$\frac{d\langle n\rangle}{dt} \approx P^{tot}_{\langle n\rangle} + \langle n\rangle \times N_p \times f^0 \left[k^{00}_{\langle n\rangle} \times f^0 + k^{0-}_{\langle n\rangle} \times f^-\right]. \quad (2)$$

Here, the second term on the right-hand side describes the increase of $\langle n\rangle$ due to coagulation (with value $f_0 = 1$ for $t > \tau_{res}$), and the first term describes the growth of $\langle n\rangle$ due to the sticking of monomers to particles with total probability $P^{tot}_{\langle n\rangle}$ (in s^{-1}). Here,

$$\begin{aligned} P^{tot}_{\langle n\rangle} &= f_0 \times P_{\langle n\rangle} + f_- \times P^-_{\langle n\rangle} + f_0 \times P^{RA}_{\langle n\rangle}, \\ P_{\langle n\rangle} &= N_1 \times k^{RR}_{\langle n\rangle}; \quad P^{RA}_{\langle n\rangle} = N_1^- \times k^{RA}_{\langle n\rangle}; \\ P^-_{\langle n\rangle} &= N_1 \times k^{AR}_{\langle n\rangle} + [M] \times k^{AM}_{\langle n\rangle}, \end{aligned} \quad (3a)$$

where N_1 and N_1^- are the monomer concentrations of main monomers (neutral and negatively charged, respectively), and [M] is the concentration of SiH_4-related molecules. $k_{\langle n\rangle}^{RR}$, $k_{\langle n\rangle}^{RA}$, $k_{\langle n\rangle}^{AR}$, and $k_{\langle n\rangle}^{AM}$ are the rate coefficients given in Ref. 26. Note that usually $[SiH_3] \approx N_1 \gg N_1^- \equiv [SiH_3^-]$ and $k_{\langle n\rangle}^{AM} \ll k_{\langle n\rangle}^{RR}$, $k_{\langle n\rangle}^{AR}$. Therefore, collisions of particles with SiH_4 and negatively charged monomers practically have no influence on particle growth and, with good accuracy, we can use the formula

$$P_{\langle n\rangle}^{tot} \approx (f_0 \times k_{\langle n\rangle}^{RR} + f_- \times k_{\langle n\rangle}^{AR}) \times N_1. \tag{3b}$$

The critical dimension n^* of cluster radicals Si_nH_m has an important role in particle production. For clusters with $n > n^*$, the association process (sticking of monomer to cluster) predominates over its diffusion losses and escapes by gas flow drag. We identify such clusters as nanoparticles. The equation obtained in Refs. 26 and 27 for n^* was

$$P_{n*}^{tot} = n* \times W_{n*}^{tot}. \tag{4}$$

The critical dimension n^* determines the rate of particle production J_{n*}. To calculate it, we need to know the concentration of clusters with critical dimension n^*. For that, we have to calculate the concentrations of all clusters with dimension $n < n^*$. The equation for concentration of neutral and negatively charged clusters can be expressed as

$$\frac{dN_n^{tot}}{dt} = \left(P_{n-1}^{tot} \times N_{n-1}^{tot} - P_n^{tot} \times N_n^{tot}\right) - W_n^{tot} \times N_n^{tot}, \tag{5}$$

where

$$P_n^{tot} = \frac{1}{1+\alpha_n}\left[P_n + P_n^{RA} + \alpha_n \times P_n^-\right];$$
$$W_n^{tot} = \frac{1}{1+\alpha_n}\left[W_n + \alpha_n \times W_n^-\right]; \quad \alpha_n = \frac{N_n^-}{N_n}. \tag{6}$$

The analytical solution of Eq. (5) for $2 \le n \le n*$ and considering quasi stationary conditions, i.e., when $dN_n^{tot}/dt \approx 0$, is

$$N_n^{tot} \equiv N_n + N_n^- \approx N_1 \times \prod_{i=2}^{n} \frac{P_{i-1}^{tot}}{P_i^{tot} + W_i^{tot}}. \tag{7}$$

From here, the concentration N_{n*}^{tot} and rate J_{n*} of particle generation can be easily calculated. The approximate analytical expression for $J_{n*} = P_{n*}^{tot} \times N_{n*}^{tot}$ obtained from Ref. 28 appears as

$$J_{n*} \approx P_{n*}^{tot} \times N_1 \times \prod_{i=2}^{n*} \frac{P_{i-1}^{tot}}{P_i^{tot}} \times \prod_{i=2}^{n_1-1} \frac{P_i^{tot}}{W_i^{tot}} \times \exp\left\{-3x_1^3 \times \Phi(x_1, x*)\right\} \tag{8a}$$

where

$$\Phi(x_1, x*) \approx 1 - \frac{1}{x_1} + \frac{1}{3x_1^2} - \frac{x_1}{x*} + \frac{x_1}{(x*)^2} - \frac{x_1}{3(x*)^3};$$
$$x_1 = 2 \times \left(\frac{W_1^{tot}}{k_1^{RR} \times [SiH_3]}\right)^{1/4};$$
$$x* \approx \frac{\sqrt{1 + 4 \times \alpha_1 \times x_1^4} - 1}{2 \times \alpha_1};$$
$$\alpha_1 \approx \frac{P_1^{att}}{P_1^{rec}} = \frac{N_e \times k_1^{att}}{N^+ \times k_1^{rec}} \ll 1. \tag{9a}$$

Here, the points x_1 and $n_1 \approx (x_1 - 1)^3$ correspond to the value $W_{n_1}^{tot}/P_{n_1}^{tot} = 1$ and, what is more, $n_1 < n*$. Values k_1^{att} and k_1^{rec} (in cm^3/s, see Ref. 26) are rate coefficients for electron attachment to SiH_3 and electron-ion dissociative recombination. If the inequality $W_1^{tot} \ge 2.2 \times k_1^{RR} \times [SiH_3]$ is applicable, we have $n_1, n* \ge 3$, It should be noted that the value $[SiH_3]$ increases with discharge power (at relatively small power, when losses of SiH_3 into nanoparticles are not important). The W_1^{tot} value decreases when gas pressure increases. Therefore, the inequality $W_1^{tot} \ge 2.2 \times k_1^{RR} \times [SiH_3]$ is usually performed at low discharge power P, gas pressure p, and relative concentration $X_{SiH_3}^0$. This has been carried out previously as experiments[2–5] and theoretical analyses.[26–28] The opposite case,

$$W_1^{tot} < 2.2 \times k_1^{RR} \times [SiH_3], \tag{10}$$

is often placed at the beginning of the discharge, and at relatively high values of P, p, and $X_{SiH_3}^0$. Experiments in the present work have mainly been conducted in such conditions, therefore in agreement with the inequality (10). However, this case requires a modification of our kinetic model.

First of all, using Eq. (10), the formulas (8a) and (9a) can be simplified

$$J_{n*} \approx P_1^{tot} \times [SiH_3] \times \exp\left\{-3 \times x_1^3 \times \Phi(x_1)\right\}, \tag{8b}$$

$$\Phi(x_1, x*) \approx \Phi(x_1) \approx 1 - \frac{1}{x_1} + \frac{1}{3x_1^2} - \frac{1}{x_1^3} + \frac{1}{x_1^7} - \frac{1}{3x_1^{11}} \quad \text{at} \quad x_1 \ge 1,$$
$$\Phi(x_1) = 0 \quad \text{at} \quad x_1 \le 1. \tag{9b}$$

Note that the value J_{n*} in Eq. (8b) at $x_1 \le 1$ is the rate of formation of clusters with critical dimension $n* = 2$, i.e., dimer-radicals. The function $\exp\left\{-3 \times x_1^3 \times \Phi(x_1)\right\} < 1$ at $x_1 > 1$ takes into account the decrease in J_{n*} due to the increase in $n*$ to values greater than 2. It can be seen that the rate (8b) for particle generation is not dependent on α_1, i.e., on negatively charged components (negative clusters). This can be understood, if we consider that the concentration of negative cluster-dimers is much lower than that of neutral ones. This case of high gas pressure and high discharge power is different from that already reported using low pressure and low power.[2–5,26–28] The influence of negative groups on particle formation rises with the growth of critical dimension n^* and can become important.[6,26–29] In previously

published cases,[2–5,26–28] where $n^* > 100$, the influence of temperature on J_{n*} was very strong. In the present case and considering Eq. (10), where $n^* = 2$, the influence of gas temperature on rate J_{n*} is weaker. Note that the rate J_{n*} of particle generation will decrease some time after discharge switching-on due to the decrease in $[SiH_3]$ and increase in parameter x_1 (see Eqs. (8b), (9a), and (9b)). This arises by the incorporation of SiH_3 radicals into growing particles. As a result, the particle concentration will reach some maximal value.

The other change in the model[26–28] is related to the rate $P_1^{tot} \times N_1$ in Eq. (8b). In fact, this must be the maximal rate of production of cluster-dimers. Detailed chemical analyses[20,21,30] have shown that SiH_3–SiH_3 collisions do not lead to the formation of Si_2H_m dimer-radicals. These dimers can be obtained due to the SiH_2 radical. Thus, in the context of our "one-step model" of cluster formation,[26–28] the first step in cluster production (i.e., the formation of dimers-radicals) is exclusively controlled by SiH_2. This determines the significant role of the SiH_2 radical in the chain of events leading to the formation of clusters and nanoparticles, which is confirmed by experimental data[8,9,11,12] and has also been reported in Ref. 20. For simplicity, calculations of SiH_2 concentration were not carried out in the first model.[26–28] However, we included these calculations in the present study. According to Refs. 12 and 30, the important channel for producing Si_2H_m dimers-radicals is the reaction[30,31]

$$SiH_2 + SiH_3 \rightarrow Si_2H_5 \quad k_{R1} \approx 3.77 \times 10^{-13} cm^3 s^{-1} \quad (R1)$$

However, the reaction (R1) is not the only one. If go out "one step approximation"[26–28] and look at the chemistry of the discharge in more detail, we can see that there are additional channels for producing dimers-radicals (see below processes (R5), (R11), (R13), and (R16)).

We should emphasise that both SiH_2 and SiH_3 radicals play an important role in the generation of nanoparticles, but SiH_2 radicals are not important for nanoparticle growth. Indeed, SiH_2 radicals are effectively attached to the other clusters and nanoparticles, which can be an important reason for SiH_2 losses, but SiH_2 concentration is much lower than that of SiH_3 and particle growth is mainly controlled by SiH_3 radical monomers.

To calculate SiH_3 and SiH_2 concentrations more precisely as well as those for the additional rates of producing radical-dimers in discharge, we also considered other neutral components such as SiH_4, Si_2H_6, H, H_2, and metastable Ar^* atoms. In this way, in addition to Eq. (R1), the following physical-chemical processes in the plasma bulk were included in the model

$$SiH_4 + e \rightarrow SiH_3 + H + e \quad k_{R2} \approx 0.9 \times \sqrt{8 \times T_e/\pi \times m_e} \times 3.3 \times 10^{-16} \times \exp\{-8/T_e\}, \quad (R2)$$

$$SiH_4 + e \rightarrow SiH_2 + 2H + e \quad k_{R3} \approx 0.1 \times \sqrt{8 \times T_e/\pi \times m_e} \times 3.3 \times 10^{-16} \times \exp\{-8/T_e\}, \quad (R3)$$

$$Si_2H_6 + e \rightarrow SiH_4 + SiH_2 + e \quad k_{R4} \approx 0.7 \times \sqrt{8 \times T_e/\pi \times m_e} \times 10^{-15} \times \exp\{-10.2/T_e\}, \quad (R4)$$

$$Si_2H_6 + e \rightarrow Si_2H_4 + H_2 + e \quad k_{R5} \approx 0.3 \times \sqrt{8 \times T_e/\pi \times m_e} \times 10^{-15} \times \exp\{-10.2/T_e\}, \quad (R5)$$

$$H_2 + e \rightarrow H + H + e \quad k_{R6} \approx \sqrt{8 \times T_e/\pi \times m_e} \times 10^{-16} \times \exp\{-14.7/T_e\}, \quad (R6)$$

$$Ar + e \rightarrow Ar^* + e \quad k_{R7} \approx \sqrt{8 \times T_e/\pi \times m_e} \times 1.6 \times 10^{-16} \times \exp\{-11.55/T_e\}, \quad (R7)$$

$$SiH_4 + SiH_2 \rightarrow Si_2H_6 \quad k_{R8} \approx 1 \times 10^{-10}, \quad (R8)$$

$$SiH_4 + H \rightarrow SiH_3 + H_2 \quad k_{R9} \approx 2.7 \times 10^{-12}, \quad (R9)$$

$$SiH_3 + H \rightarrow SiH_2 + H_2 \quad k_{R10} \approx 2.5 \times 10^{-11} \times \exp(-2500/T_g), \quad (R10)$$

$$Si_2H_6 + SiH_3 \rightarrow SiH_4 + Si_2H_5 \quad k_{R11} \approx 1 \times 10^{-12}, \quad (R11)$$

$$Si_2H_6 + H \rightarrow SiH_4 + SiH_3 \quad k_{R12} \approx 1.1 \times 10^{-12}, \quad (R12)$$

$$Si_2H_6 + H \rightarrow Si_2H_5 + H_2 \quad k_{R13} \approx 2.2 \times 10^{-12}, \quad (R13)$$

$$SiH_4 + Ar^* \rightarrow SiH_3 + H + Ar \quad k_{R14} \approx 0.9 \times 4 \times 10^{-10}, \tag{R14}$$

$$SiH_4 + Ar^* \rightarrow SiH_2 + 2H + Ar \quad k_{R15} \approx 0.1 \times 4 \times 10^{-10}, \tag{R15}$$

$$Si_2H_6 + Ar^* \rightarrow Si_2H_4 + 2H + Ar \quad k_{R16} \approx 6.6 \times 10^{-10}, \tag{R16}$$

$$H_2 + Ar^* \rightarrow 2H + Ar \quad k_{R17} \approx 7 \times 10^{-11}. \tag{R17}$$

All rate coefficients in Eqs. (R2)–(R17) are given in $cm^3 s^{-1}$.[30,32–35] In Eq. (R10), T_g is gas temperature in K and $\sqrt{8 \times T_e/\pi \times m_e}$ is the average velocity of plasma electrons (m_e is electron mass).

It can be seen from this list of processes that, in addition to Eq. (R1), other sources of radical-dimers in our model are the processes (R5), (R11), (R13), and (R16). Hence, the rate $P_1^{tot} \times N_1$ in formula (8b) must be replaced by a summation of the rates of processes (R1), (R5), (R11), (R13), and (R16). Note that these processes (with the exception of Eq. (R1)) are carried out with disilane (Si_2H_6) molecules, which, in turn, are produced in reaction (R8) with SiH_2.

In addition to Eqs. (R14) to (R17), the loss of metastable Ar^* can also be due to collisions with nanoparticles and diffusion at the wall. Losses by collisions with particles can be described by the probability (in s^{-1}) $N_p \times \pi \times (R_p + R_{Ar})^2 \times \langle v_{p-Ar} \rangle$, where R_p and R_{Ar} are the radius of the particle and that of the Ar atom, respectively, and $\langle v_{p-Ar} \rangle$ is the average velocity of the colliding particles and Ar atoms.

For a correct calculation of [SiH_2], [SiH_3] and the rate of particle generation, J_{n*}, we need to know the values of branching ratios of SiH_4 dissociation by electrons and Ar^*. In the case of dissociation by electrons, different values of branching ratios can be found in the literature. For SiH_2 production, a minimal value 0.1 was used (see first factor in Eq. (R3)),[30,32] which provides better agreement with the measured low SiH_2 concentrations in silane-Ar discharges.[8,9,12] For the case of dissociation by Ar^*, the measured values of branching ratios are not known and, for SiH_2, we also used a low value (≈ 0.1) (see Eq. (R15)).

In addition to the losses of particles and SiH_3 at the surface (with transport by diffusion from the volume to the surface), similar losses and those due to leakage of gas flow were also taken into account for all other neutral species. The formula for probabilities of losses at the surface by diffusion transport is given in Ref. 27. The probability of losses through leakage (in s^{-1}) is equal to $1/\tau_{res}$, where τ_{res} is the resident time for the neutral species in the discharge. Dimensionless values of the probability of loss in a collision of SiH_3, H, SiH_2, and Ar^* with the wall were taken as 0.16, 0.16, 1, and 1, respectively. In the case of collision with particles, the dimensionless values were 0.6, 0.6, 1, and 1, respectively. These probabilities were zero for H_2 and Si_2H_6.

To determine the average particle dimension $\langle n \rangle$, particle concentration N_p and concentration of the species SiH_4, SiH_3, SiH_2, Si_2H_6, H, and Ar^*, eight balance equations, time-dependent and coupled (including Eqs. (1) and (2)), were solved. The concentration of H_2 molecules in the discharge was determined from the condition of constant gas pressure, i.e., equality $[H_2] \approx [SiH_4]^0$-[SiH_4]-[SiH_3]-[SiH_2]-[Si_2H_6]-[H], where $[SiH_4]^0$ is the silane concentration at the inlet (initial).

The condition of neutrality of the plasma

$$N_e + Z_p \times N_p = N^+ \tag{11}$$

as well as the simplified stationary balance equation for N^+ and the absorption of electric power P (see Ref. 27) were used to calculate the electron concentration N_e and temperature T_e, and the concentration of positive ions N^+. In Eq. (11), the Z_p value is the average negative charge of particles (expressed in units of electron charge, e). This average charge and fraction f_0 of neutral particles were found from the charge distribution function (CDF) for particles with diameter D_p. CDF was calculated according to Refs. 36 and 37, taking into account the quantum nature of charges. For rough estimations, the following analytical formulas can be used for Z_p and f_0:[36]

$$Z_p \approx 0.35 \times D_p \times T_e \times \ln\left(29.8 \times \delta \times \frac{N_e}{N^+} \times \frac{D_p}{Z_p} \sqrt{T_e \times T_+ \times M_+}\right),$$

$$f_0 \approx \left(\frac{1.44}{\pi \times D_p \times T_e}\right)^{1/2} \times \exp\left(-1.44 \times \frac{1}{D_p \times T_e} \times Z_p^2\right). \tag{12}$$

Here, δ is the sticking coefficient for electron attachment to particle with diameter D_p (in nm), M_+ is the mass of positive ions (in atomic units), while electron and ion temperatures, T_e and T_+, are given in eV. We assumed that $T_+ \approx T_g$, where the average gas temperature T_g was calculated from the stationary equation of thermal conductivity and the fact that approximately 20% of the total power, absorbed by the discharge, was used to heat the gas.

Finally, in the simplest approach, the linear diameter of the particles D_p is related to the "dimension" $\langle n \rangle$ by the expression:

$$D_p = D_1 \times \langle n \rangle^{1/3}, \tag{13}$$

where D_1 is the linear diameter of a monomer. This relation means that the particle mass density is independent on the particle diameter. However, in our case, the particles have a dense core and porous shell.[27] Hence, in the present model, we took into account this effect and D_p was calculated as a function of $\langle n \rangle$.

In conclusion, we should note that the kinetic model presented here was suitable for the study of the conditions in which the relative initial SiH_4 concentration X^0_{SiH4} could reach as high as 100% (in contrast to our previous model,[26–28] where $X^0_{SiH4} \leq 10\%$). Such a conclusion is the consequence of Eqs. (3), (4), (8b), (9b), and (10). When the

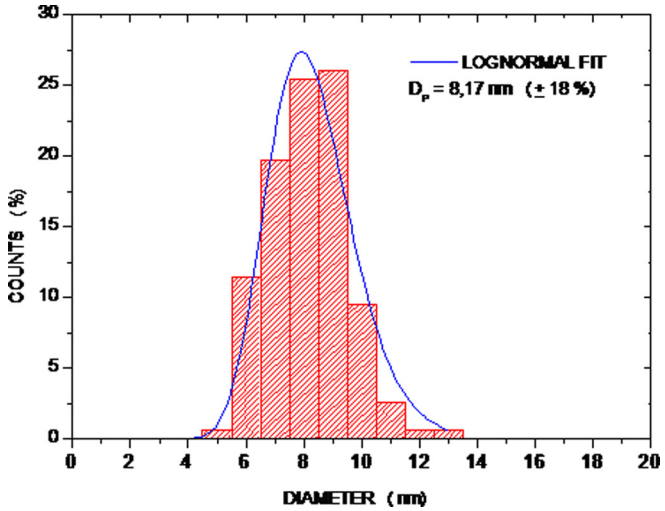

FIG. 2. (Color online) Particle dimension distribution for a discharge of 40 Pa, 200 W, 158 sccm, 5% SiH_4, and pulses of 200 ms.

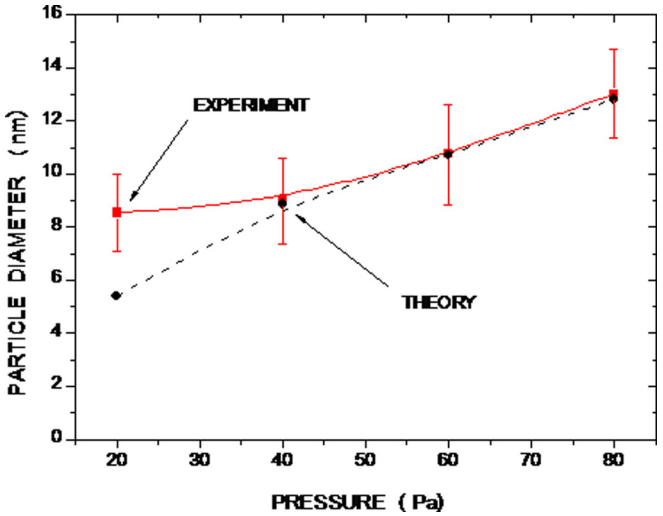

FIG. 4. (Color online) Dependencies of particle diameter on gas pressure at time = 200 ms, $P = 200$ W, $Q = 158$ sccm, and $X_{SiH4} = 0.0759$ (■ and full line—experiment; • and dashed line – model calculation).

discharge switches on at high discharge power, the SiH_4 concentration is reduced due to high dissociation. Therefore, $[SiH_3]$ can reach the same order of magnitude as $[SiH_4]$. In such conditions, the second part of the formula for $P^-_{\langle n \rangle}$ (see (3a)) is not important at any X^0_{SiH4} value and, therefore, formulas (3b), (4), (8b), (9b), and (10) are independent of X^0_{SiH4}.

IV. MEASUREMENTS AND MODEL CALCULATIONS: COMPARISON AND DISCUSSION

Experiments were performed in an RF capacitive discharge with frequency 13.56 MHz as described in Sec. II. The used discharge parameters were: discharge power P, gas pressure p, gas flow rate Q, and relative inlet concentration X^0_{SiH4}. The studied ranges were: $P = 40$ to 200 W, $p = 20$ to 80 Pa, $Q = 40$ to 220 sccm, and $X^0_{SiH4} = 0.05$ to 0.14. Electrodes worked at room temperature $T_w \approx 293$ K and absorbed power was higher than 90% from P. After finishing a series of discharge pulses, the nanoparticles were collected from substrates located outside the plasma box. The nanoparticles were then examined by transmission electronic microscopy (TEM), providing the size of the particles and their size distribution.

Some experimental results are shown in Figs. 2 to 8. A typical particle dimension distribution (PDD) is presented in Fig. 2.

Fig. 2 shows that particles typically have a lognormal-shaped PDD with relatively small dispersion. The kinetic model described in this work does not provide the PDD. Therefore, we only considered the average particle diameters D_p in order to compare.

Dependencies on gas flow rate Q are given in Fig. 3. We observed that acceptable agreement between experimental measurements and model calculations were more marked at higher values of gas flow rate.

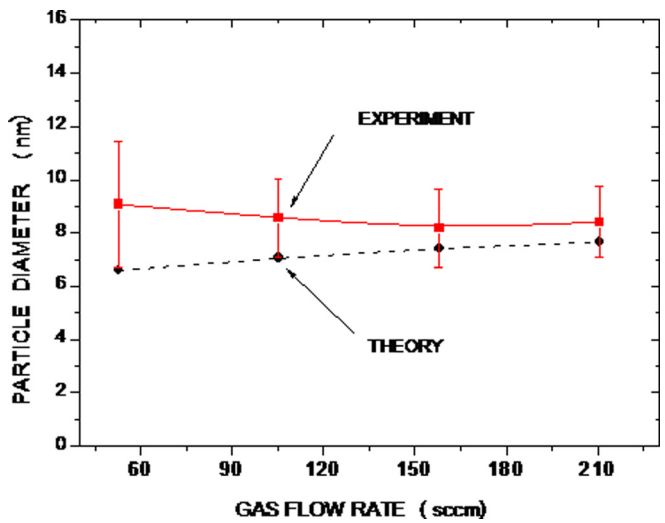

FIG. 3. (Color online) Dependencies of particle diameter on total gas flow rate at time = 200 ms, $p = 40$ Pa, $P = 200$ W, and $X_{SiH4} = 0.051$ (■ and full line—experiment; • and dashed line – model calculation).

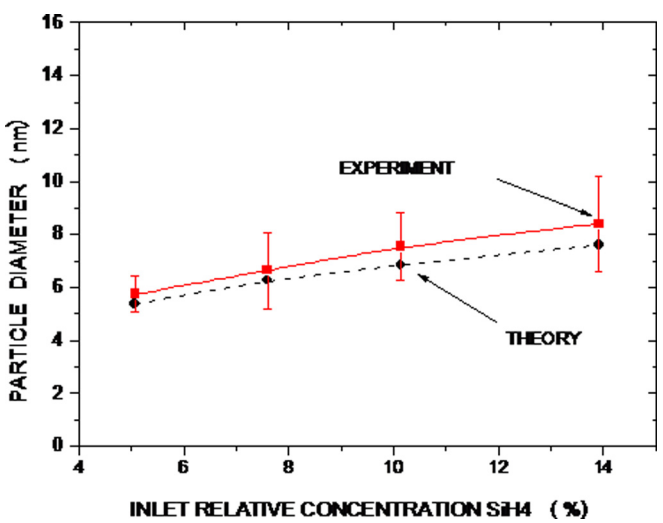

FIG. 5. (Color online) Dependencies on X^0_{SiH4} of D_p at time = 50 ms, $p = 40$ Pa, $Q = 158$ sccm, and $P = 200$ W (■ and full line—experiment; • and dashed line — model calculation).

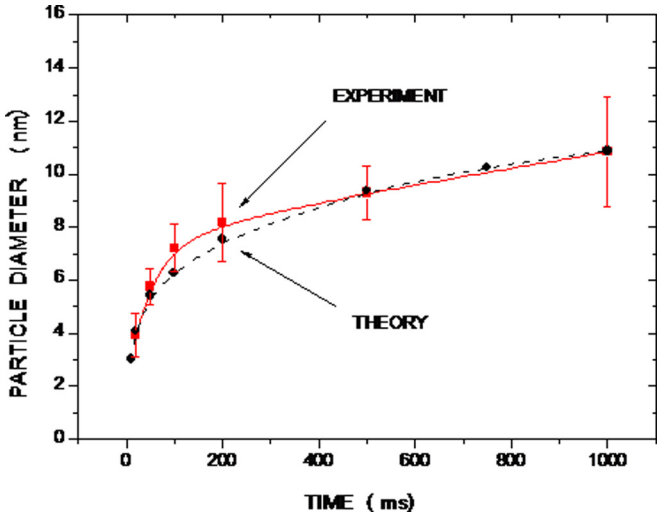

FIG. 6. (Color online) Measured and calculated dependencies on time of discharge-on of particle diameter at $P = 200$ W, $p = 40$ Pa, $Q = 158$ sccm, and $X_{SiH4} = 0.0506$ (■ and full line—experiment; • and dashed line – model calculation).

Dependencies on gas pressure are presented in Fig. 4 and also show agreement between experimental data and theory at $p \geq 40$ Pa. The growth of D_p with an increase in gas pressure can be explained by an increase in particle concentration N_p. In fact, the increase in N_p facilitates particle coagulation and, consequently, growth of particle dimension. Discrepancy between measurement and calculation at low pressure $p = 20$ Pa could be because parameter $x_1 > 1$ and condition (10) are not satisfied at the beginning of the "discharge-on." At low pressure, $\Phi(x_1) > 0$ and J_{n*} becomes small (see Eqs. (8b) and (9b)) and as a result, N_p becomes relatively low and particle diameter due to coagulation also decreases.

The dependencies of particle diameter D_p as a function of inlet relative concentration X^0_{SiH4} are given in Fig. 5. Experimental data and model calculations show good agreement.

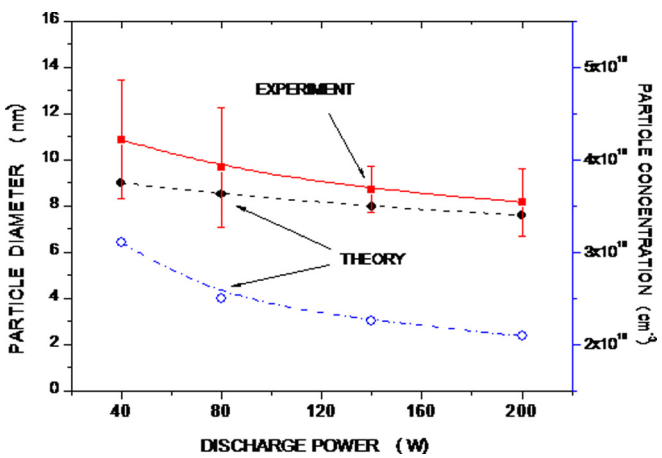

FIG. 7. (Color online) Dependencies of particle diameter (filled symbols) and concentration (empty circles) on discharge power for time = 200 ms, $p = 40$ Pa, $Q = 158$ sccm, and $X_{SiH4} = 0.051$ (■ and full line—experiment; •, ○, and dashed or dotted-dashed lines – model calculation).

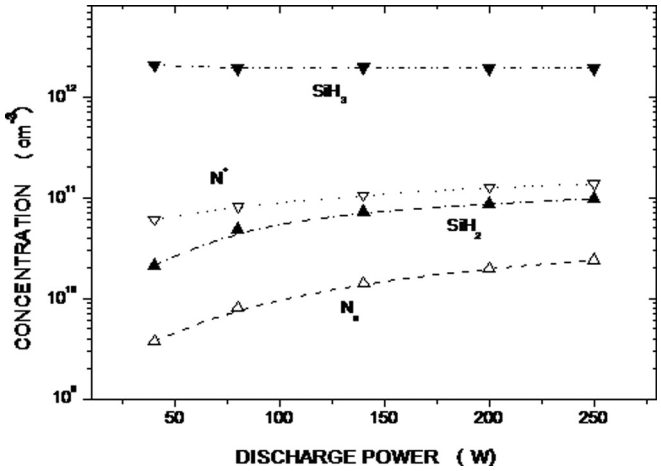

FIG. 8. Dependencies on discharge power of concentrations SiH_3, SiH_2, positive ions N^+, and electrons N_e for a time of 100 ms at $p = 40$ Pa, $Q = 158$ sccm, and $X_{SiH4} = 0.051$.

Measurements and calculations of time dependencies of particle diameter D_p with all the other fixed parameters are presented in Fig. 6. The theory confirmed the non-linear behavior of experimental time dependency. Growth is mainly managed by the contribution of coagulation because particle concentration is big. For $t > \tau_{res} = 0.12s$, the coagulation is the only growth process. Note that here, the time dependency of particle diameter was smoother than that of $t^{0.4}$ for pure coagulation of neutral particles.[7,27] This is through additional decreasing of particle concentration due to diffusion losses.

Dependencies on discharge power of particle diameter are shown in Fig. 7.

Fig. 7 shows a monotonous decrease in particle diameter with increasing power P. The physical reason for this was interpreted on the basis of the decrease in particle concentration. This decrease is due to the increase in gas temperature and, consequently, a decrease of time when the particle production rate J_{n*} remains high (see Eqs. (8b) and (9b)).

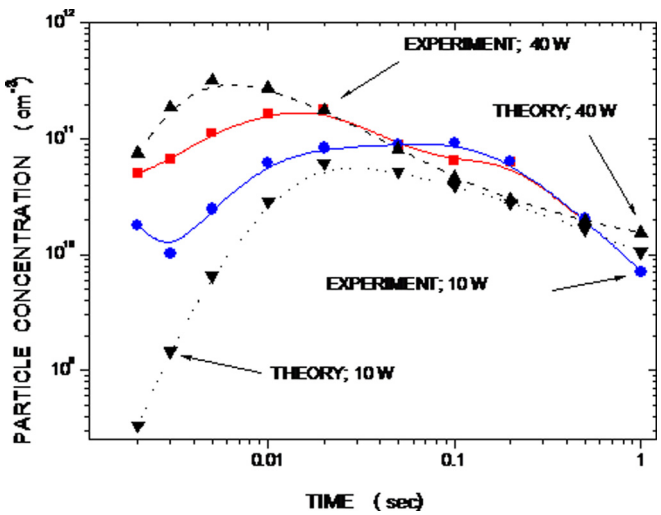

FIG. 9. (Color online) Measured and calculated dependencies on time of particle concentrations at $P = 10$ and 40 W, $p = 13$ Pa, $Q = 20$ sccm (at $P = 10$ W), and 5 sccm (at $P = 40$ W) for discharge in pure silane (squares, circles, and full lines—experiment (Ref. 12); triangles, dashed and dotted lines - - -, ···, our model calculation).

One of the advantages of this theoretical analysis is the possibility of estimating the concentration of the main species present in the plasma. We have presented the calculated concentrations of $[SiH_2]$, $[SiH_3]$, N^+, and N_e in Fig. 8, though experimental measurements were not carried out in the present study.

We also compared particle concentrations N_p, calculated from our model for the conditions described for the experiment reported in Ref. 12, with the experimental values obtained in this work for RF discharge in pure silane. For this, we made a small change in Eq. (1), taking into account the geometry of the discharge in Ref. 12. We assumed that 30% of the discharge power was transformed into gas heat. This comparison is presented in Fig. 9. Acceptable agreement between our theory and the measurements appears for time ≥ 0.01 s. Discrepancies for shorter times could be due to low experimental accuracy (more than one order of magnitude of values[12]) and, above all, that condition (10) was not satisfied at the beginning of the discharge-on.

V. CONCLUSION

Experimental and theoretical investigations of nanoparticle growth in SiH_4-Ar RF discharge were carried out at gas pressure between 20 and 80 Pa, discharge power 40 to 250 W, gas flow rate 40 to 220 sccm, and relative inlet SiH_4 concentration 0.05 to 0.12. The growth of particle diameter was not linear with time. The reason for this non-linear dependency is mainly due to particle coagulation. The distinctive feature of the presented kinetic model is that it contains (just as our previously published models[26–28]) some important parameters, such as critical dimension n^* and rate of particle generation J_{n*}. This permits the calculation of particle concentration and, therefore, allows us to interpret quantitatively the particle growth. For this, we used the analogy of the classical kinetic theory of condensation of supersaturated vapors. The studied model for relatively high gas pressure and discharge power (when $x_1 \leq 1$, see Eq. (10)) corresponds to the case of strongly super-saturated vapour of SiH_3 at the initial period after the discharge-on, when the critical dimension is minimal ($n^* = 2$). Such a model can be useful for describing the kinetics of generation and growth of other kinds of nanoparticles and nanostructures (e.g., nanowires or nanoparticles with different compositions).

ACKNOWLEDGMENTS

This work was supported by the program *Ajuts a la Recerca de la Facultat de Física de la Universitat de Barcelona,* CTQ2009-14674-C02-01 of MICINN (Government of Spain), 2009SGR00185 of AGAUR (Generalitat de Catalunya) and the Network *Plasma en Materiales Poliméricos*, MAT2006-26547-E, coordinated by the *Universitat Politècnica de Catalunya*. One of the authors, M.J.I.I., acknowledges the PhD grant supported by CONICYT (Government of Chile). The authors thank the Serveis Cientifico-tècnics of the Universitat de Barcelona (SCT-UB) for measurement facilities.

[1]*Dusty Plasmas*, edited by A. Bouchoule (Wiley, New York, 1999).
[2]L. Boufendi, A. Plain, J. Ph. Blondeau, A. Bouchoule, C. Laure, and M. Toogood, Appl. Phys. Lett. **60**, 169 (1992).
[3]A. Bouchoule and L. Boufendi, Plasma Sources Sci.Technol. **2**, 204 (1993).
[4]L. Boufendi, J. Hermann, A. Bouchoule, B. Dubreuil, E. Stoffels, W. Stoffels, and M. de Giorgi, J. Appl. Phys. **76**, 148 (1994).
[5]L. Boufendi and A. Bouchoule, Plasma Sources Sci.Technol. **3**, 262 (1994).
[6]Ch. Hollenstein, J.-L. Dorier, J. Dutta, L. Sansonnens, and A. Howling, Plasma Sources Sci. Technol. **3**, 278 (1994).
[7]C. Courteille, Ch. Hollenstein, J.-L. Dorier, E. Bertran, G. Viera, R. Martins, and A. Macarico, J. Appl. Phys. **80**, 2069 (1996).
[8]Y. Watanabe, M. Shiratani,T. Fukuzawa, H. Kawasaki, Y. Ueda, S. Singh, and H. Ohkura, J. Vac. Sci.Technol. A **14**(3), 995 (1996).
[9]H. Kawasaki, K. Sakamoto, S. Maeda, T. Fukuzawa, M. Shiratani, and Y. Watanabe, Jpn. J. Appl. Phys. Part 1 **37**, 5757 (1998).
[10]M. Shiratani, T. Fukuzama, and Y. Watanabe, Jpn. J. Appl. Phys. Part 1 **38**, 4542 (1999).
[11]Y. Matsuoka, M. Shiratani, T. Fukuzawa, Y. Watanabe, and K-S. Kim, Jpn. J. Appl. Phys. Part 1 **38**, 4556 (1999).
[12]T. Fukuzama, S. Kushima, Y. Matsuoka, M. Shiratani, and Y. Watanabe, J. Appl. Phys. **86**, 3543 (1999).
[13]G. Viera, S. Huet, E. Bertran, and L. Boufendi, J. Appl. Phys. **90**, 4272 (2001).
[14]G. Viera, M. Mikikian, E. Bertran, P. Roca i Cabarrocas, and L. Boufendi, J. Appl. Phys. **92**, 4684 (2002).
[15]Z. Shen, T. Kim, U. Kortshagen, P. H. McMurry, and S. A. Campbella, J. Appl. Phys. **94**, 2277 (2003).
[16]I. B. Denysenko, K. Ostrikov, S. Xu, M. Y. Yu, and C. H. Diong, J. Appl. Phys. **94**, 6097 (2003).
[17]C. S. Kim, W. K. Youn, and N. M. Hwang, J. Appl. Phys. **108**, 014313 (2010).
[18]M. Shigeta and T. Watanabe, J. Appl. Phys. **108**, 043306 (2010).
[19]U. Kortshagen and U. Bhandarkar, Phys. Rev. E: Stat. Phys., Plasmas, Fluids, Relat. Interdiscip. **60**, 887 (1999).
[20]U. Bhandarkar, M. Swihart, S. Girshik, and U. Kortshagen, J. Phys. D: Appl. Phys. **33**, 2731 (2000).
[21]U. Bhandarkar, U. Kortshagen, and S. Girshik, J. Phys. D: Appl. Phys. **36**, 1399 (2003).
[22]K. de Bleecker, A. Bogaerts, R. Gijbels, and W. Goedheer, Phys. Rev. E: Stat. Phys., Plasmas, Fluids, Relat. Interdiscip. Top. **69**, 056409, (2004); K. De Bleeker, A. Bogaerts, and W. Goedheer, Phys. Rev. E: Stat. Phys., Plasmas, Fluids, Relat. Interdiscip. Top. **70**, 056407 (2004).
[23]A. Fridman, L. Boufendi, T. Hbid, B. Potapkin, and A. Bouchoule, J. Appl. Phys. **79**, 1303 (1996).
[24]D. Lemons, R. Keinigs, D. Winske, and M. Jones, Appl. Phys. Lett. **68**, 613 (1996).
[25]A. Gallagher, Phys. Rev. E: Stat. Phys., Plasmas, Fluids, Relat. Interdiscip. Top. **62**, 2690 (2000).
[26]B. Gordiets and E. Bertran, Chem. Phys. Lett. **414**, 423 (2005).
[27]B. Gordiets and E. Bertran, Russ. J. Phys. Chem. **2**, 315 (2008).
[28]B. Gordiets and E. Bertran, Tech. Phys. **54**, 674 (2009).
[29]S. Choi and M. Kushner, J. Appl. Phys. **74**, 853 (1993).
[30]M. Kushner, J. Appl. Phys. **63**, 2532 (1988).
[31]M. Coltrin, R. Kee, and A. Miller, J. Electrochem. Soc. **133**, 1206 (1986).
[32]J. Perrin, J. P. M. Schmitt, G. De Rosny, B. Drevillon, J. Huc, and A. Lloret, Chem. Phys. **73**, 383 (1982).
[33]V. Rusanov and A. Fridman, *Physics of Chemically Active Plasma* (Nauka, Moscow 1984) (in Russian).
[34]G. Inoue and M. Suzuki, Chem. Phys. Lett. **122**, 361 (1985)
[35]E. Meeks, R. S. Larson, P. Ho, C. Apblett, S. M. Han, E. Edelberg, and E. S. Aydil, J. Vac. Sci. Technol. A **16**, 544 (1998).
[36]B. Gordiets and C. M. Ferreira, J. Appl. Phys. **84**, 1231 (1998).
[37]B. Gordiets and C. M. Ferreira, J. Appl. Phys. **86**, 4118 (1999).